LA-UR-07-0992

Title: VALIDATION SPECIMEN FOR CONTOUR METHOD
EXTENSION TO MULTIPLE RESIDUAL STRESS
COMPONENTS

Author(s): Pierluigi Pagliaro (WT-2)
Michael B. Prime (WT-2)
Bernardo Zuccarello (University of Palermo)
Bjørn Clausen (LANSCE-LC)
Thomas R. Watkins (Oak Ridge National Laboratory)

Los Alamos
NATIONAL LABORATORY
—— EST.1943 ——

VALIDATION SPECIMEN FOR CONTOUR METHOD
EXTENSION TO MULTIPLE RESIDUAL STRESS COMPONENTS

P. Pagliaro[a,b], M.B. Prime[b], B. Zuccarello[a], B. Clausen[b] and T.R. Watkins[c]

[a] Dipartimento di Meccanica, Universitá degli Studi di Palermo, Palermo 90128, Italy, pagliaro@dima.unipa.it
[b] Los Alamos National Laboratory, Los Alamos, NM 87544, USA, prime@lanl.gov
[c] High Temperature Materials Laboratory, Materials Science and Technology Division, Oak Ridge National Laboratory, Oak Ridge, TN 37831, USA

ABSTRACT

A new theoretical development has been made that will allow the contour method to measure a cross-sectional map of not just the normal stress but all three normal stress components. To validate this development, a residual stress test specimen was designed, fabricated and then tested with different experimental techniques. A 60-mm diameter $\times$10-mm thick disk of 316L stainless steel was plastically compressed through the thickness with a 15 mm diameter flat indenter in the center of the disk to provide a unique biaxial stress state that is ideal for testing the theory. The stresses in the specimen were first mapped using time-of-flight neutron diffraction. Next, the hoop stresses were mapped on a cross-section using the contour method, and the agreement with the neutron measurements was excellent. The extension of the contour method to multiple components requires the measurement of in-plane stresses on the cut surface, after electrochemical removal of material affected by the cut. An initial attempt to measure the in-plane stresses using x-ray diffraction was unsuccessful because of the large grain size of the material. Further attempts will be made using hole drilling. A finite element prediction of the stresses from the indentation process gave reasonable agreements with the data but was limited in its accuracy because the 316L showed a Bauschinger effects that has not yet been correctly modelled. The indented specimen makes an excellent residual stress test specimen, and suggestions for improving the specimen are given.

1. INTRODUCTION

Residual stresses play a significant role in many material failure processes like fatigue, fracture, stress corrosion cracking, buckling and distortion. Residual stresses are the stresses present in a part free from any external load, and they are generated by virtually any manufacturing process. Because of their important contribution to failure and their almost universal presence, the knowledge of residual stress is crucial for prediction of the strength of any engineering structure. A massive research effort is focused on this task. However, the knowledge of residual stresses is a very complex problem. In fact, the development of residual stress generally involves nonlinear material behavior, phase transformation, coupled mechanical and thermal problems and/or varying mechanical properties throughout the material. Hence, the ability to accurately quantify residual stresses through measurement is an important engineering tool.

Recently, a new method for measuring residual stress, the contour method [1, 2], has been introduced. With the contour method, a part is carefully cut in two along a flat plane causing the residual stress normal to the cut plane to relax. The contour of each of the opposing surfaces created by the cut is then carefully measured. The deviation of the surface contours from planarity is assumed to be caused by elastic relaxation of residual stresses and is therefore used to calculate the original residual stresses. One of the unique strengths of this method is that it provides a full cross-sectional (two-dimensional) map of the residual stress component normal to the cross section. Other common methods that can provide similar 2-D stress maps have significant limitations. The neutron diffraction method is nondestructive and is capable of producing full 3D stress maps, but it is sensitive to microstructural changes [3], time consuming, and limited in maximum specimen size, about 50 mm, and spatial resolution, about 1 mm. Conventional sectioning methods [4] are experimentally cumbersome, analytically complex, error prone, and have limited spatial resolution, about 1 cm. Other relaxation methods, at least those that are commonly used, determine at most a one-dimensional depth profile [5], although some can measure multiple stress components [6]. On the other hand, a limitation of the contour method is that only one residual stress component is determined from the measurement. DeWald and Hill [7] proposed an extension of the contour method for the measurement of multiple stress components by making cuts at 45 degrees from the first cut plane, using the hypothesis of a continuously processed body. An approach to reconstruct multiple components of the original residual stress on different cut planes by making multiple cuts was demonstrated in [8].

This paper describes the design, analysis and construction of a test specimen to validate a theoretical extension of the contour method to allow the measurement of orthogonal stress components on the same cut plane. Preliminary measurements on the specimen are reported but not the complete measurements to validate the new theory. The proposed extension of the contour method is described and involves using multiple techniques in order to reconstruct the other stress components on the cut plane. The residual stress field was introduced in the cylindrical plate test specimen by indentation of cylindrical tools on each side of the specimen under controlled conditions. This method to introduce residual stresses in a specimen was also used by Mahmoudi et al. [9] for a somewhat different purpose, so the design here is different. The residual stresses were predicted by means of a finite element (FE) model of the indentation process. Neutron diffraction measurements were carried out in order to measure the residual stresses introduced and to validate the FE prediction and eventually the contour method measurements. Then, a contour method test was executed by cutting the specimen along the plane scanned by neutron diffraction. To verify the multiple components theory, x-ray diffraction measurements were attempted on the cut surface of the specimen. The paper concludes by comparing the measurements and prediction and assessing the suitability of the indentation process as a mechanism to introduce known residual stress fields into test specimens.

In the future, several hole-drilling tests will be executed on the same indented specimen on the cut surfaces, so the residual stress relaxed by the cut will be measured in order to validate the multiple residual stress components theory presented in this paper.

2. THEORY

In order to motivate the design of the test specimen, the theories for both the traditional contour method and the extension to multiple stress components are presented.

2.1 Conventional Contour Method

Before introducing the new theory for multiple stress components, the original theory for only one stress component is reviewed. The contour method [1, 2] is based on a variation of Bueckner's superposition principle [10]. Figure 1 presents an illustration in 3-D of the contour method.
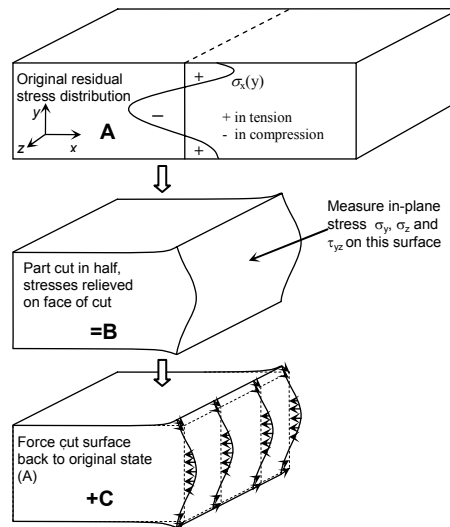

Figure 1 – *Superposition principle to calculate residual stresses from surface contour measured after cutting the part in two.*

In **A**, the part is in the undisturbed state containing the residual stress to be determined. In **B**, the part has been cut in two and has deformed because of the residual stresses released by the cut. In **C**, the free surface created by the cut is forced back to its original flat shape. Superimposing the stress state in **B** with the change in stress from **C** gives the original residual stress throughout the part, as shown by the following expression:

$$\sigma^{(A)} = \sigma^{(B)} + \sigma^{(C)} \tag{1}$$

This superposition principle assumes elastic relaxation of the material and that the cutting process does not introduce stress that could affect the measured contour. The contour of the free surface is experimentally measured after the cut and the surface of a stress-free model is analytically forced back to its original flat configuration by applying the opposite of the measured contour as boundary conditions. This is usually done using FEM. Because the partially relaxed stresses in **B** are generally unknown, one cannot obtain the original stress throughout the body. However, the normal and shear stresses on the free surface in **B** must be zero (σ_x, τ_{xy} and τ_{xz}). Therefore, step **C** by itself will give the correct stresses along the plane of the cut:

$$\sigma_x^{(A)} = \sigma_x^{(C)}$$
$$\tau_{xy}^{(A)} = \tau_{xy}^{(C)} \tag{2}$$
$$\tau_{xz}^{(A)} = \tau_{xz}^{(C)}$$

In practice, only the normal stress component σ_x, can be experimentally determined. The experimental measurement of the contour only provides information about the displacements in the normal (x) direction, not those in the transverse (y) direction. Therefore, the surface is forced back to the original flat configuration (step **C**) in the x-direction only. The shear stresses (τ_{xy} and τ_{xz}) are constrained to zero in the solution. The stress-free constraint is automatically enforced in most implicit, structural, finite-element analyses if the transverse displacements are left unconstrained. Even if residual shear stresses were present on the cut plane, averaging the contours measured on both halves of part still lead to the correct determination of the normal stress σ_x [1].

A small convenience is taken in the data analysis by finite element modeling. Modeling the deformed shape of the part for step **C** in Figure 1 would be tedious. Instead, the surface is initially flat in the finite element model, and then the part is deformed into the shape opposite of the measured contour. Because the deformations are quite small, the same answer is obtained but with less effort.

2.2 Reconstruction of Multiple Stress Components

Once the part has been cut in two and the original σ_x residual stress on the cut plane is obtained, it is also possible to determine the other original residual stresses on same cut plane ($\sigma_y^{(A)}$, $\sigma_z^{(A)}$ and $\tau_{yz}^{(A)}$). The same finite element calculation that determines the original $\sigma_x^{(C)}$ residual stress in the cut plane also determines how much the in-plane stress components on the cut plane were changed by the relaxation from the cut, $\sigma_y^{(C)}$, $\sigma_z^{(C)}$ and $\tau_{yz}^{(C)}$. After the cut, the post-relaxation in-plane stresses ($\sigma_y^{(B)}$, $\sigma_z^{(B)}$ and $\tau_{yz}^{(B)}$) can be measured by a surface technique such as x-ray diffraction or hole drilling, see Figure 1, after electrochemical removal of material affected by the cut process. A simple summation with the results of the previous finite element calculation (Eq. 1) then provides the original components of the residual stress on the plane that was cut.

$$\sigma_y^{(A)} = \sigma_y^{(B)} + \sigma_y^{(C)}$$
$$\sigma_z^{(A)} = \sigma_z^{(B)} + \sigma_z^{(C)} \tag{3}$$
$$\tau_{yz}^{(A)} = \tau_{yz}^{(B)} + \tau_{yz}^{(C)}$$

3. SPECIMEN DESIGN AND FABRICATION

In order to validate the theoretical development, a test specimen was designed to provide a residual stress distribution particularly well suited for this purpose. It was desired to test the contour method on different stress states where the two significant normal stress components were approximately equal (i,e., equi-biaxial) and, conversely, of opposite sign. Such a stress state can be produced in a shrink-fit ring and plug, in which the expansion of a cooled, oversized plug is constrained by a surrounding ring resulting in biaxial compressive residual stresses in the plug. The ring experiences compressive radial stresses under the forces from the plug, but the hoop stresses are tensile. However, since a real ring and plug would fall apart during contour method cutting, an alternative configuration to produce a similar residual stress distribution was used. A circular disk was plastically compressed through the thickness by two cylindrical indenters of smaller diameter [9], see Figure 2(a). The compressed region between the two indenters yields and wants to expand in the radial direction due to the Poisson effect. Under the constraint of the surrounding material, analogous to the ring in the example of a shrink-fit ring and plug, a biaxial (hoop and radial) compressive residual stress state is produced in the central region, while in the outer region there will be a tensile and compressive residual stress state for hoop and radial stresses, respectively (see Figure 2(b)).
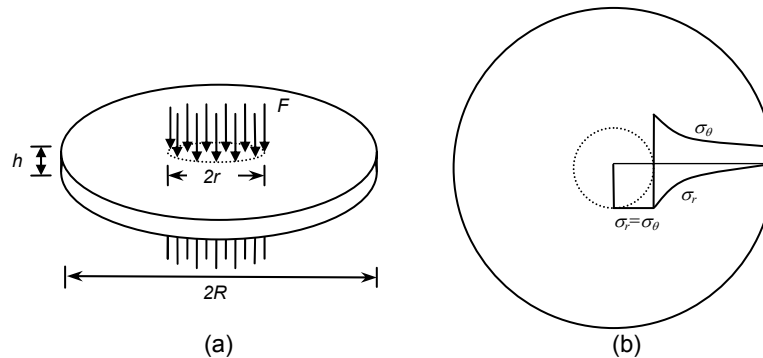

Figure 2 – Schematic diagram illustrating (a) the indentation process, (b) the ideal residual stress distribution obtained.

316L stainless steel was chosen for the material as the best compromise among the ideal materials for the different measurement methods that will be required to validate the multiple-component theory. For the contour method, hole drilling, and other relaxation methods, it is generally better to have a material with high σ_y/E in order to obtain more relaxation (contour and strains). So for this reason aluminum would be a good choice, but unfortunately, it is not as good for x-ray diffraction measurements. Austenitic steel has a lower σ_y/E, which means lower relaxed strains, but it is very good for neutron diffraction and x-ray diffraction. 316L stainless steel was chosen based on previous successful diffraction measurements and industrial importance. The disk was machined from a square cross-hot rolled plate (457 mm x 457 mm and 12.7 mm thickness) of 316L stainless steel. The chemical composition of the 316L Stainless steel is in weight percents: C=0.018, Mn=1.59, P=0.031, S=0.005, Si=0.23, Ni=10.64, Cr=16.65, Mo=2.16, N=0.05 and Fe=balance (in accord with the ASTM A240 and ASME SA-240). In order to eliminate the presence of any preexisting residual stresses, the plate was annealed at 1050 °C for 30 minutes in vacuum and then cooled to room temperature in argon. After annealing, a metallographic analysis was made on the plate to check the grain-size (see Figure 3), whose average is about 50-100 μm, with some smaller grains. The metallography also revealed the presence of about 0.5% ferrite, seen as dark stringers, which is not enough to cause any multi-phase problems with the diffraction measurements of residual strains. A small amount of ferrite is typical in 316L stainless.
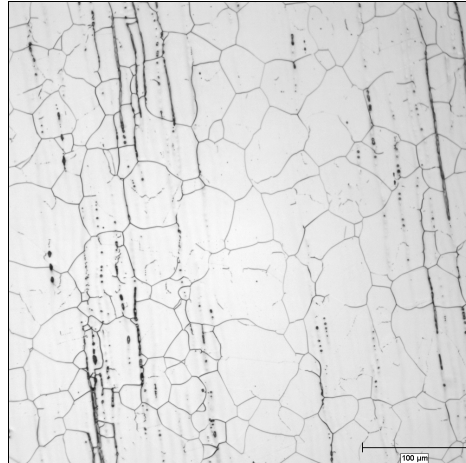

Figure 3 – Metallography of the 316L plate after annealing. The scale bar is 100 μm long.

A preliminary experimental program to determine the mechanical properties of the material was carried out. Several compression tests, in accord with ASTM standard, were carried out in order to test the mechanical behavior of the material in the through-thickness direction and in the two rolling directions. Three cylindrical specimens, 9.5 mm in diameter and 12.7 mm height, were extracted from the plate. Displacement-control compression tests with a crosshead speed of 0.046 mm/min were executed until ~20% of engineering strain and then unloaded. The rate was chosen to give approximately the same strain rate as was expected during the specimen indentation. Figure 4 shows the true stress – true strain curves for the three tested material directions. The three curves are very close; however, the material is slightly softer in the x-direction. From the slope of the linear part (unloading) of these curves the Young's modulus, *E*, was found to be 193 GPa while the yield stress σ_y is 185 MPa. The linear part of the curve during loading gave a Young's modulus lower than the expected value for this steel. However, after few consecutive load-unload cycles in the elastic range, the linear loading curve rose to the expected value. Probably, the annealing process resulted is some plasticity at very low loads.
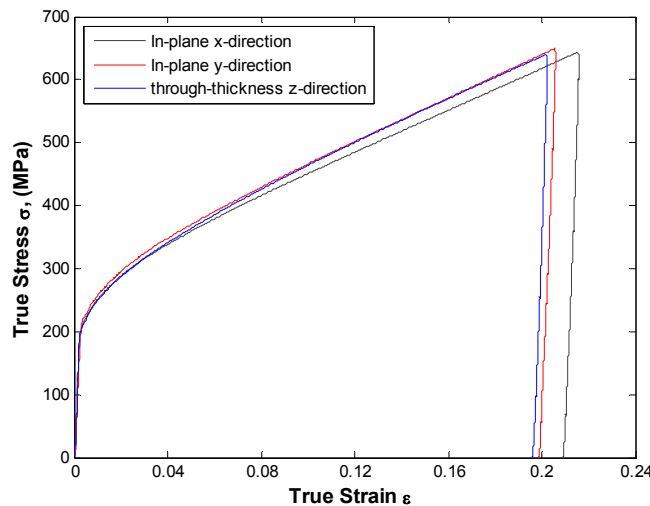

Figure 4 – Stress – true strain curves of uniaxial compression tests for the 316L stainless steel.

The geometry of the specimen was then designed considering the constitutive behavior and experimental limitations. A 60 mm diameter ×10 mm thick disk of 316L stainless steel was chosen with the indenters 15 mm in diameter, see Figure 5. The thickness was chosen based on the limited penetration of neutrons, while the diameters of the disk and the indenters were chosen to obtain stress gradients that could be resolved using reasonable neutron sampling volumes, to obtain a relaxed contour of at least 20 μm (peak to valley) and also considering the maximum load of the test machine. The indenters were also designed by means of several finite element simulations in order to minimize the stress concentrations, since there are some fillet radii. The indenter material used was an A2 tool steel, characterized by a high hardness (64 HRC) and a high yield stress (about 1300 MPa). The Young modulus of A2 tool is 204 GPa with a Poisson's ratio of 0.3. In order to center the two indenters with respect to the disk, two PMMA rings were designed (see Figure 5), which are moved out of the way prior to indentation.
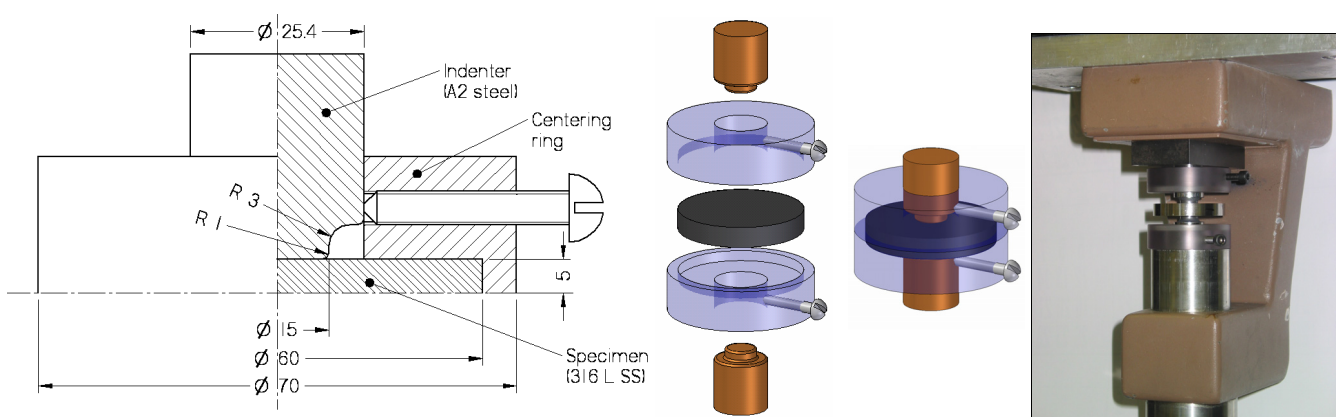

Figure 5 – *Design of the indentation fixture and photo of the indentation fixture and specimen in the load frame.*

The specimen was indented to a peak load of 90 kN under displacement control using a crosshead speed of 0.15 mm/min. A MOLYCOTE® Anti-Friction Coating was applied on the contact surfaces of the two indenters. A footprint in both side of the disk was produced with a thickness reduction of -0.85%. Since the displacement measurement (blue curve in Figure 6) is affected by the compliance of the specimen, the indenters, the lubricant and part of the test machine, due to the position of the sensor, a preliminary test without any specimen (indenter versus indenter) was executed to the same maximum load to measure the in series compliance of the indenters-lubricant-test machine (green curve in Figure 6). By subtracting the measured displacements of the two tests, the displacements at the indenter-specimen interface were obtained (red curve in Figure 6).
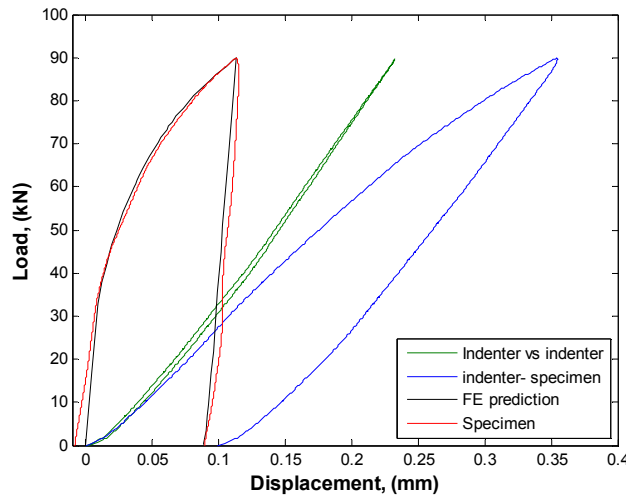

Figure 6 – *Load – displacement curves of the indentation process and FE prediction.*

4. RESIDUAL STRESS PREDICTION

The residual stress field produced by the indentation was simulated using the ABAQUS finite element code [11]. Figure 7 shows the layout of the FE analysis. An axisymmetric model of 1/2 of the specimen was built using 15,000 four-node quadrilateral elements (CAX4R) with reduced integration. Square elements 0.1 mm on a side gave a 50 × 300 mesh in the disk for 15,000 elements. The indenter was modeled using the same element type but with a coarser mesh of 8,725 elements about 0.2 mm on a side. The contact behavior between the indenter (master surface) and the specimen (slave surface) was

assumed frictionless because the lubricant was used during the experimental test, and a surface-to-surface contact algorithm was used. Axial-symmetric boundary conditions were imposed along the axis of the indenter and the specimen, while symmetric boundary conditions were imposed on the middle plane of the specimen. A displacement of about -0.10 mm was applied at the upper face of the indenter (the actual cross-head displacement is the double due to the symmetry) to achieve the applied load of -90 kN, which is in agreement with experimentally applied load.
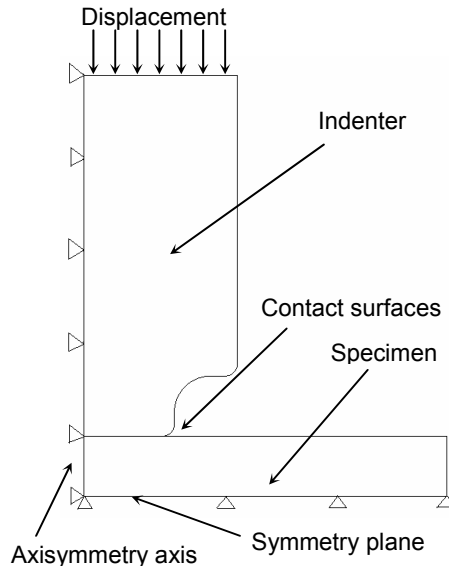

Figure 7– Details of the axial-symmetric finite element model used showing the planes of symmetry.

The material properties shown in Figure 4 were averaged and used to model the behavior of the 316L stainless steel. The A2 tool steel was modeled by assuming linear elastic behavior, since the stresses do not approach yield during indentation.

Because it was discovered that 316L stainless steel exhibits a Bauschinger effect [12, 13], and the indentation process produces some reverse loading effect in the central region, different hardening models were used in the FE prediction. In detail, both isotropic and combined hardening models were used for preliminary simulations. For the isotropic hardening model, the half-cycle of the available stress-strain curve (Figure 4) was used, while for the combined hardening model the parameters were automatically obtained by ABAQUS evaluating the best fit of the half-cycle stress-strain curve. Since no experimental data were available yet for the backstress evolution in this particular plate, parameters available in literature were used [13]. In the future some reverse loading tests will be executed in order to get the correct parameters for the combined hardening model. Figure 8 shows the FE prediction of the residual stress over the diametrical cross section of the disk for both isotropic and combined hardening models.

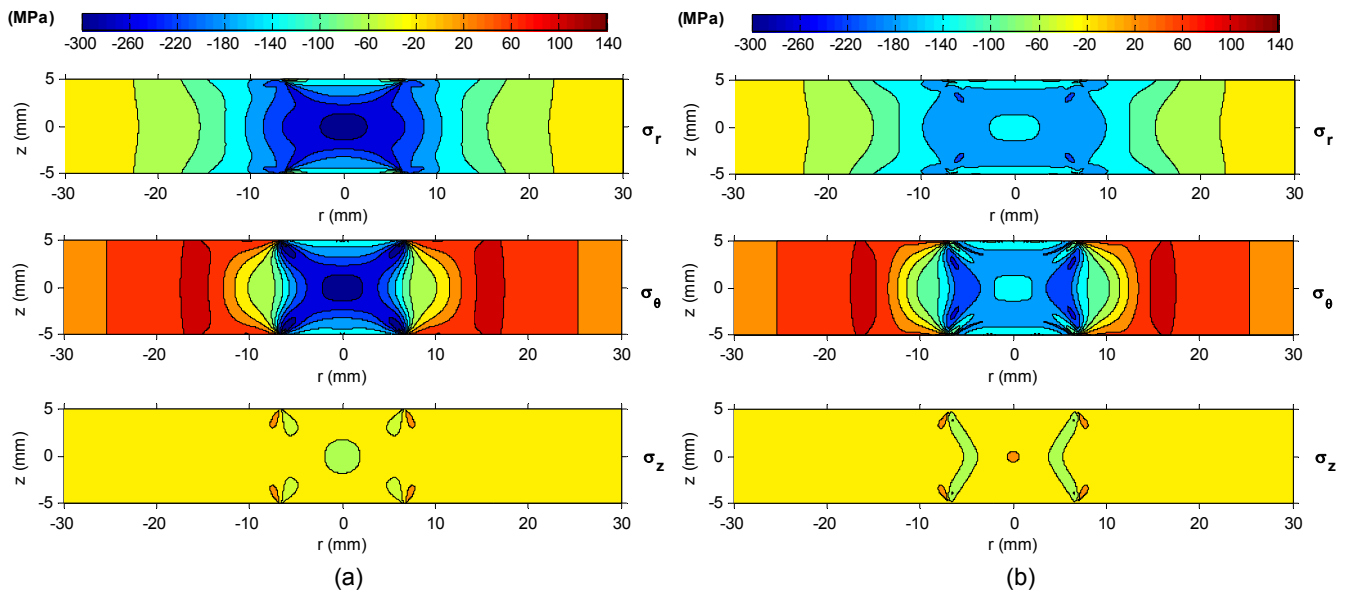(a)   (b)

Figure 8 – FEM prediction of the radial, hoop and axial residual stresses along the diameter plane using (a) an isotropic hardening model and (b) a combined hardening model.

5. EXPERIMENTS

5.1 Neutron diffraction

The neutron diffraction (ND) measurements were made using the SMARTS instrument at Los Alamos Neutron Science Center (LANSCE). LANSCE is a pulsed neutron source where the neutrons are generated by accelerating protons in a linear accelerator and bombarding them into a tungsten target. Every time a proton pulse hits the target a burst of neutrons is generated by spallation. Each pulse of neutrons contains a spectrum of wavelengths and is moderated by passing through a chilled water moderator at 10 °C. The incident flight path on SMARTS is 31 meters, most of it in a neutron guide. SMARTS has two detector banks at plus and minus 90 degrees to the incident beam with a diffracted flight path length of about 1.5 m, see Figure 9(a). The total flight path, the scattering geometry and the 20 Hz repetition rate of the source dictates that the useable wavelength range on SMARTS is about 0.4 to 3.8 Å with maximum intensity between 0.5 to 1.5 Å.

A typical diffraction pattern for the 316L stainless steel from this study is shown in Figure 9(b). As seen in Figure 9(b), many peaks from the austenitic stainless steel are present enabling Rietveld full pattern analysis [14]. Being able to use multiple peaks in the refinement greatly improves the statistics, and using the GSAS software [15] we can determine the lattice parameter, a, of the fcc crystal structure with a relative accuracy of about 50×10^{-6}, or 50 microstrain ($\mu\varepsilon$), using count times on the order of 20 minutes. The incident slits were set to 2×2 mm^2, and a set of radial collimators limited the gauge volume to 2 mm along the incident beam path. The sample was positioned so that the scattering vector for the +90 degrees bank, Q_1, was along the axial (z) direction, and the scattering vector for the -90 degrees bank, Q_2, was along the radial (r) direction of the cylindrical sample. A series of measurements were made on a diameter plane by first scanning along the direction of Q_2. Then the sample was rotated 90 degrees around the axial direction, and another scan was performed in the vertical (out of the plane of the paper in Figure 9(a)) direction. Hence the first and second scans were made in the same physical positions within the sample, but in the first scan the *radial* strains, ε_r, were measured in the -90 degrees bank, and in the second scan the *hoop* strains, ε_θ, were measured in the -90 degrees bank. In both scans the axial strains, ε_z, were measured in the +90 degrees bank. Further measurements were also executed on an un-indented disk specimen, so supposedly stress free.

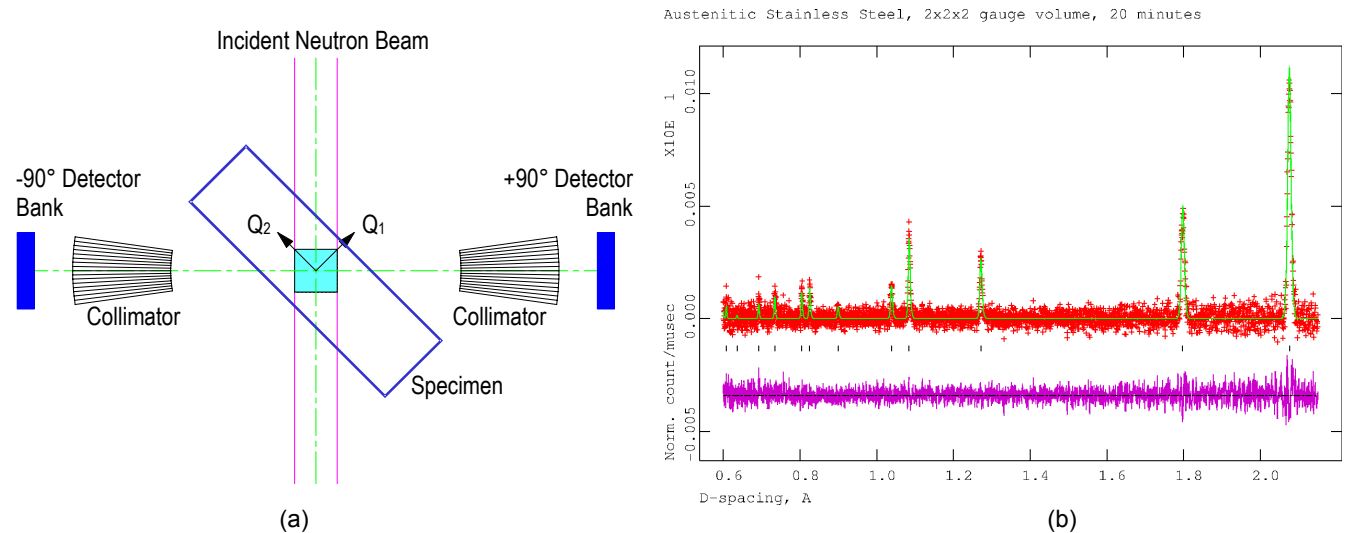|	
(a)	(b)

Figure 9 – (a) Schematic setup of SMARTS for spatially resolved measurements, and (b) Typical diffraction pattern. The red crosses are the data, the green line is the Rietveld refinement and the magenta line is the difference curve. The black tick-marks indicate the positions of the face-centered cubic peaks.

The lattice strains are calculated based upon a stress-free reference measurement. In this case the average stress-free lattice parameters from a series of measurements on three small cubes (5 mm x 5 mm x 5 mm) were determined. Then the residual strains can be calculated as follows:

$$\varepsilon_i = \frac{a_i}{a_i^0} - 1 \qquad i = r, \theta, z \tag{4}$$

where a_i and a_i^0 are the stresses and unstressed lattice parameters, respectively, in the test specimen and in the stress-free cubes along the different directions (r, θ, z). Then the residual stress components were evaluated using Hooke's law:

$$\sigma_i = \frac{E(1-\nu)}{(1+\nu)(1-2\nu)} \left[\varepsilon_i + \frac{\nu}{1-\nu}(\varepsilon_j + \varepsilon_k) \right] \qquad i, j, k = r, \theta, z \tag{5}$$

where E is the elastic modulus, and ν is Poisson's ratio.

The measured lattice strains for *z* = 0 along the disk mid-thickness, are plotted in Figure 10 along with the FE predictions of the elastic strains considering either isotropic or combined hardening model.
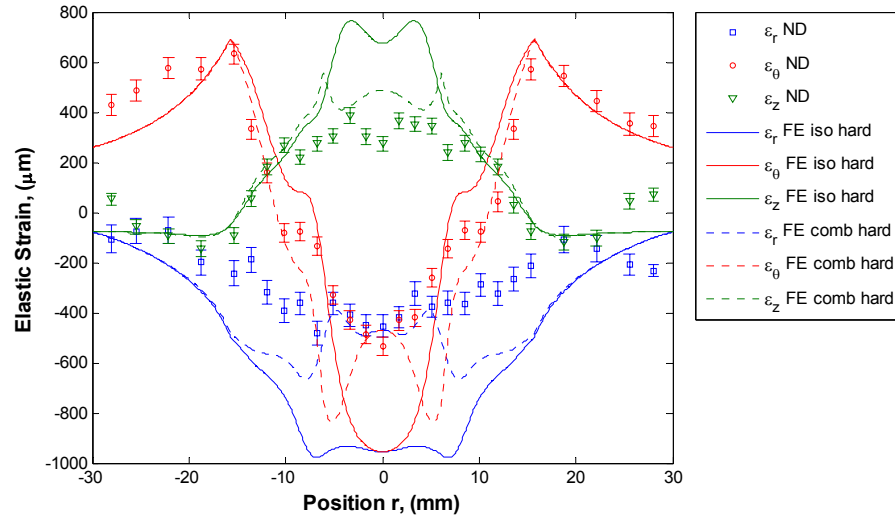

Figure 10 – *Neutron diffraction measured elastic strain along the diameter line plotted with the FE predicted elastic strains using either isotropic or combined hardening model.*

Figure 11 shows the residual stress components calculated with Eq. 5 from the neutron diffraction measured elastic strains.
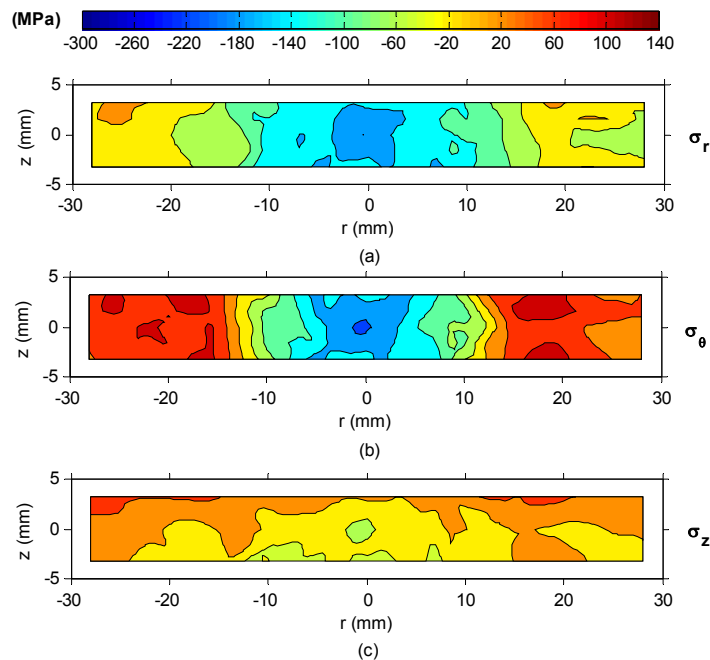

Figure 11 – *Maps of (a) radial, (b) hoop and (c) axial residual stresses measured with neutron diffraction on the diametrical plane.*

5.2 Contour method

The contour method (CM) was applied to both the indented disk and, as a control, to the unindented disk. The conventional contour method was applied to measure the hoop stress over a diametrical cross section.

The specimens were cut in half along the same planes scanned by neutron diffraction using wire electric discharge machining (EDM) and a 50 μm diameter tungsten wire. The parts were submerged in temperature-controlled deionized water throughout the cutting process. "Skim cut" settings were used. The parts were constrained by clamping on both sides of the cut to the work plate of the EDM machine (see Figure 12(a)). To prevent any thermal stresses, the specimens and the fixture were allowed to come to thermal equilibrium in the water tank before clamping. As it is possible to see from Figure 12(a), the clamp directions were parallel to the wire axis and perpendicular to the cutting direction.

After cutting the two disks, the contours of the resulting four surfaces of the disk halves were measured using a Taylor-Hobson Talyscan 250 laser scanner. A laser triangulation probe of 2 mm range and resolution of 0.1 μm was used. The cut surfaces were measured on a 0.1 mm spaced grid, giving about 60,000 points on each cut surface. As it is possible to see from Figure 12(b), the four disk halves were positioned on the work plane of the laser scan machine, aligning the axis of the halves, so the following data alignment and data reduction were easier.
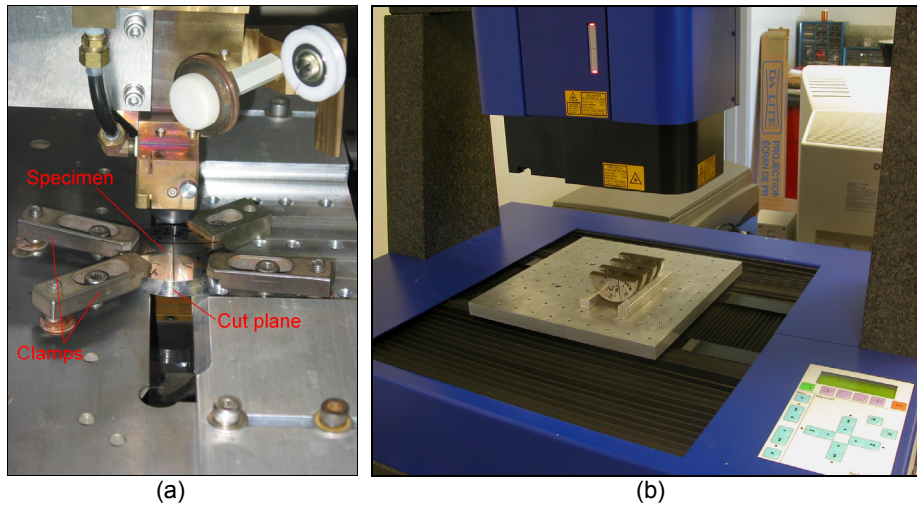

(a)   (b)

Figure 12 – *(a) EDM cut setup (b) laser scan setup.*

The raw data was processed into a form suitable to calculate stresses using a procedure described in detail elsewhere [16]. Data points from when the probe was off of the surface were removed. The two point clouds (the collection of *x,y,z* datapoints that define each surface) for each specimen were aligned in a common coordinate system, mirroring one of the two clouds with respect to the axial direction. Since the data points do not extend completely to the part edges, an extrapolation was executed by means of Delaunay triangulation with a nearest point option that uses the value of the nearest point (linear interpolation option doesn't work well in this case because it makes a triangulation between points too far from each other). Then the two clouds were averaged point by point to provide a single data set and also to minimize several potential error sources, as better described in [16]. Figure 13 shows the average of the contours measured on the two opposing surfaces created by the cut for the blank (Figure 13(a)) and the indented disk (Figure 13(b)) respectively. The peak-to-valley amplitude of the contour is about 8 μm for the blank disk and 40 μm for the indented disk.

The contour on the unindented disk was used to correct the contour on the indented disk. From Figure 13(a) it is evident that the measured contour of the blank specimen is not flat. Slitting tests (crack compliance) on the annealed 316L material indicated that the post-annealing stresses were less than 10 MPa. The neutron results in the unindented disk are consistent with these low stresses, although this low stress is difficult to measure precisely with neutrons. Therefore, the contour on the unindented disk is probably caused by the EDM cutting and not by residual stress since it would require stresses over 100 MPa to produce such a contour. The wire used had half the diameter of the smallest wire previously used for contour measurements. A lower tension must be used with smaller wire, and it is affected by vibrational bending. So, to eliminate this effect in the indented disk, the blank disk contour was subtracted from the indented disk contour (see Figure 13(c)). In retrospect, cutting with a 100 μm diameter wire would likely have given better results, and further tests to verify this are planned.
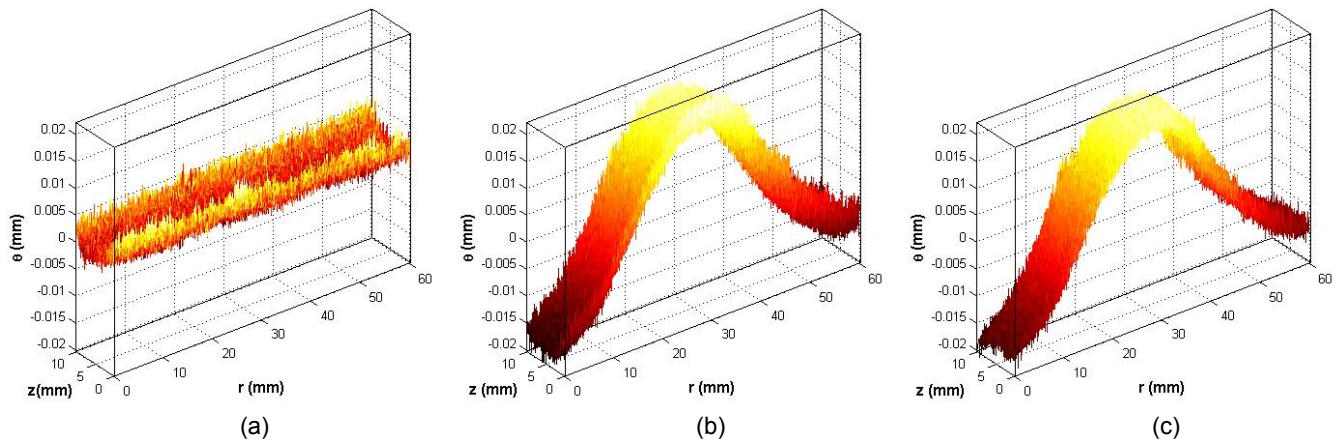

(a)   (b)   (c)

Figure 13 – *Contours of (a) blank specimen, (b) indented specimen and (c) their difference.*

The σ_θ stresses that were originally present on the cut plane were calculated numerically by elastically deforming the cut surface into the opposite shape of contour that was measured at the same surface [1]. This was accomplished using the ABAQUS commercial FE code [11] and a 3-D elastic finite element model (see Figure 14). A model of half of the disk specimen was constructed. The mesh used 51,920 linear hexahedral (8 node) elements. The material behavior was considered elastically isotropic with an elastic modulus of 193 GPa and a Poisson's ratio of 0.3. In order to smooth out noise in the measured surface data and to enable evaluation at arbitrary locations, the data were fitted to a bivariate smoothing spline. The smoothing spline fits were evaluated at a grid corresponding to the FE nodes, and those values at the nodal locations were then used as displacement boundary conditions. The results obtained are showed in Figure 15.
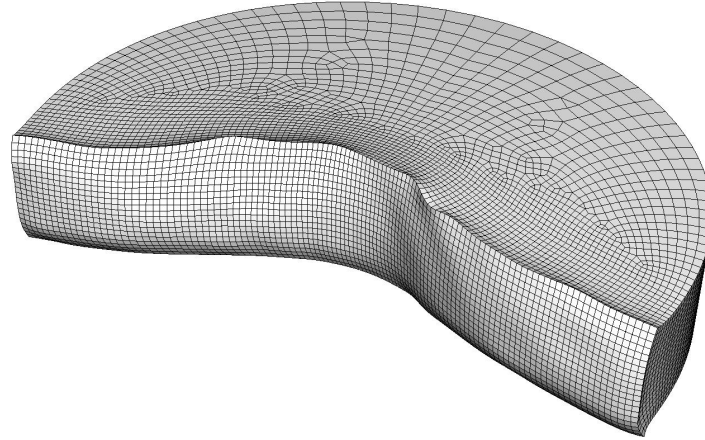

Figure 14 – *FE model of 316L stainless steel disk after cut, deformed into opposite of measured shape in order to calculate original residual stresses. Deformation magnified by 400.*
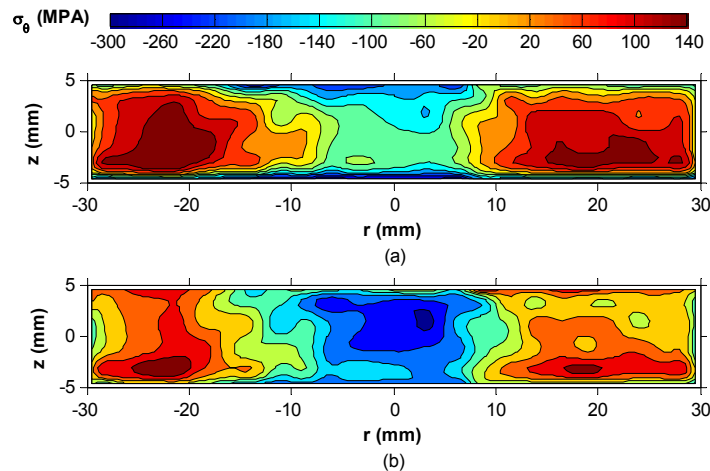

Figure 15 –*Maps of hoop residual stresses measured with the contour method: (a) uncorrected results and (b) by applying the difference between the indented and blank specimen contours.*

5.3 X-ray diffraction

X-ray diffraction (XRD) measurements were made using two types of goniometers at the High Temperature Materials Laboratory, Oak Ridge National Laboratory. Table 1 lists the details of the experimental conditions for the x-ray measurements using the first unit. Briefly, a 4-axis ($\phi, \chi, \Omega, 2\Theta$) goniometer [17] was employed for the stress measurements using the "ψ-goniometer geometry" (see Figure 16(a)) [18(a)]. The (220) and (311) reflections from the 316L austenitic steel were utilized for the strain measurement along the length of the samples using Cr $K\alpha$ and $K\beta$ radiations, respectively. Measurements were restricted to a 4 x 4 mm area by using Pb tape for masking. Given the large grain size (50-100 μm), rocking scans were performed at each nominal tilt to locate four low intensity regions; that is, sample orientations where there is minimal contribution to the intensity from a large grain or grains. The detector scans were then performed at fixed ϕ, ψ (=χ) and Ω. Additional scans were made at each of the nominal ψ values, i.e., at $\psi \pm 0.2°$ for a total of twelve scans per nominal ψ.

Specimen alignment was accomplished using a dial gauge probe which was accurate to ± 5 μm. Here, the relative distance to the center of rotation is known, and the diffracting surface is positioned accordingly. Goniometer alignment was ensured by

examining LaB$_6$ powder on a zero background plate. The maximum observed peak shift for the (510) reflection of LaB$_6$ (141.7 °2Θ) was less than 0.01° 2Θ for ψ tilting as described in Table 1.

The stresses were calculated using the Dölle-Hauk method [18(b)], assuming a biaxial stress state. For this stress state, the equation relating strain to stresses:

$$\varepsilon_{\phi\psi} = \frac{d_{\phi\psi} - d_0}{d_0} = \frac{1+\nu}{E}\sigma_\phi \sin^2\psi - \frac{\nu}{E}(\sigma_{11} + \sigma_{22}) \tag{6}$$

assuming $\sigma_{13} = \sigma_{23} = \sigma_{33} = \phi = 0$. ε, d, ν, E and σ are the strain, interplanar spacing, Poisson's ratio, Young's modulus and stress, respectively. Poisson's ratio and Young's modulus were taken as 0.3 and 193 GPa, respectively. The variables and subscripts ϕ, ψ and 0 refer to the azimuthal angle, tilt angle and strain-free, respectively. $d_{\psi=0}$ was taken as the strain free interplanar spacing, d_0.

Table 1 – *Experimental conditions of the x-ray measurements 4-axis (ϕ, χ, Ω, 2Θ) goniometer.*

Parameter	Condition
Equipment	Scintag PTS goniometer
	Spellman DF3 series 4.0 kW generator
	Scintag liquid N$_2$-cooled Ge detector
Power	1.44 kW; 40 kV, 36 mA
Radiation	Cr, λ $kK\alpha$ = 2.28970 Å, λ $kK\beta$ = 2.08487 Å
Incidence slit divergence	0.24°
Receiving slit acceptance	0.25°; radial divergence limiting (RDL) Soller slit
Source to specimen distance	290 mm
Specimen to back slit distance	290 mm
Mask and mapping locations	4 x 4 mm Pb mask, R= 0 and 25 mm
Tilt axis and nominal tilt angles	Ω; 0, ±28.2, ±42, ±55 ° (equal steps of $\sin^2\Psi$)
Scans	0.02 °2Θ/step

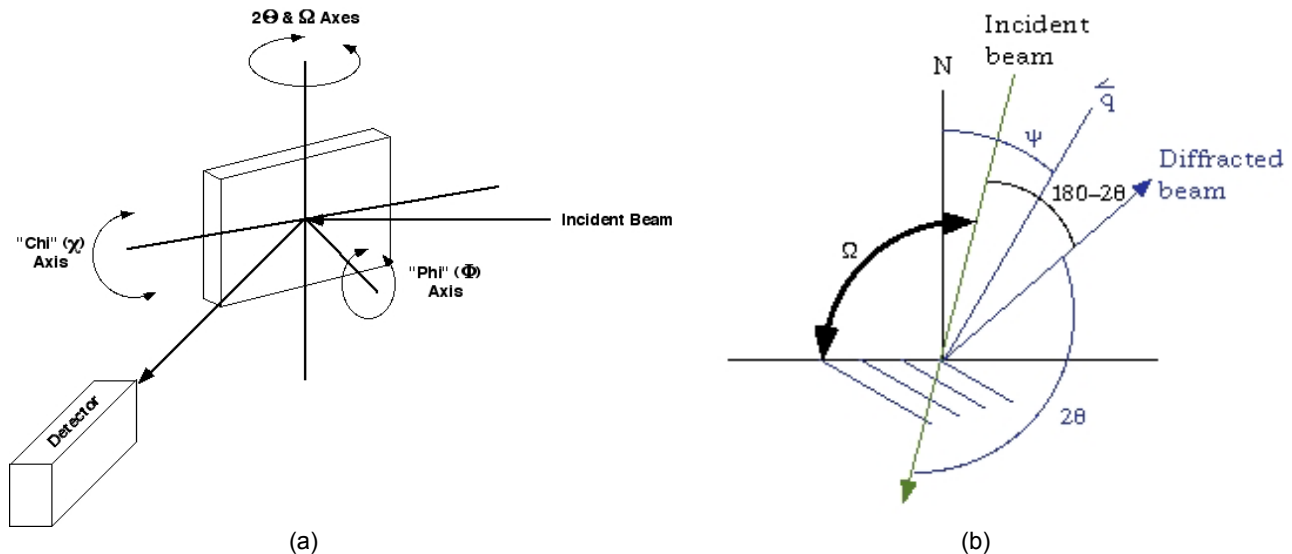(a)   (b)

Figure 16 – *(a) ψ-goniometer geometry and (b) Ω-goniometer geometry for residual stress measurements.*

Table 2 lists the details of the experimental conditions for the x-ray measurements on a second unit. Briefly, a single axis (ψ) goniometer [19] was employed for the stress measurements using the "Ω-goniometer geometry" (see Figure 16(b)) [18(c)]. The (311) reflection from the austenitic steel was utilized for the strain measurements. During scanning, the ψ axis was oscillated ±4° to improve particle statistics. Specimen alignment was accomplished using a contact probe which was accurate to ±0.25 mm. Goniometer alignment was ensured by examining a stress-free Fe powder pellet. The maximum observed peak shift for the (211) reflection of Fe (156 °2Θ) was less than 0.06 °2Θ for Ω tilting as described in Table 2.

This data was analyzed with the RSA software [20], and the stresses were also calculated using the "$\sin^2\psi$" technique [18(b)].

Parameter	Condition
Equipment	TEC Model 1600 x-ray stress analyzer
	Position sensitive detector (PSD), 14°2Θ range
Power	52.5 W; 35 kV, 0.75 mA
Radiation	Cr, λ $K\beta$ = 2.08487 Å
Source to specimen distance	220 mm
Specimen to detector distance	220 mm
Collimator	5 mm diameter
Mask and mapping locations	4 x 4 mm Pb mask, R= 0 and 25 mm
Tilt axis and angles	Ω; ψ values varied, $\pm40°$ max in equal steps of $\sin^2\psi$
Scans	0.06 °2Θ/step from 142-156°2Θ ; 180 sec/scan.

A typical peak profile of the 316L disk contained peaks from two or more grains or sets of grains (see Figure 17(a)). In an effort to avoid such peaks, the available diffracting grains were prescreened via the rocking curves described above. Scans from a particular Ω orientation and nominal ψ were then averaged and profile fit, reducing the 12 scans to four profile fit peak positions per nominal ψ. Any scans revealing any obvious "multi-grain" nature, as shown below, were excluded. The resulting ε versus $\sin^2\psi$ iṣ shown in Figure 17(b). Despite our best efforts to average and minimize the influence of the large grains (see Figure 3), this typical $\sin^2\psi$ plot shows lots of scatter due to interaction strains or elastic incompatibility strains between grains. While each individual strain measurement is valid and correct, the heterogeneity displayed indicates that it is not prudent to force the x-ray residual stress analysis further.
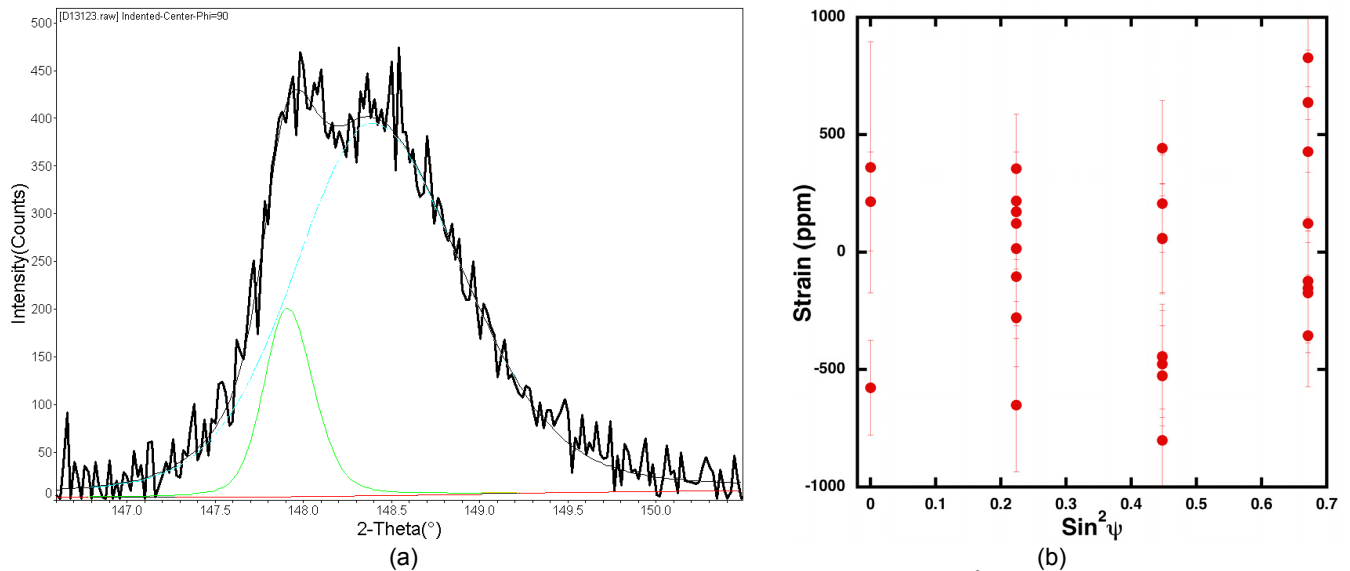

(a)   (b)

Figure 17 – (a) Typical (311) profile and (b) typical ε vs $\sin^2\psi$.

6. DISCUSSION AND FUTURE PLANS

Figure 18 shows the residual stresses measured by neutron diffraction (ND) and the FE predictions along the specimen mid-thickness. In detail, there are two set of curves for the FE predictions, one for the isotropic and one for the combined hardening model. The trends for both FE predictions are pretty close to the neutron diffraction measurements, especially in the outer region where there are no reverse loading effects. It is also evident that the shape of the isotropic hardening curves is very similar to the ND results, the only differences are in the absolute value of the stresses in the central region where a reverse loading effect is present. In contrast, the combined hardening curves have magnitudes more similar to the ND measurements but the curves have a different shape. As described in [12], the 316L stainless steel exhibits a more complicated kinematic hardening behavior than the simple ABAQUS combined model that involves two non-linear kinematic work-hardening terms. So, in order to better predict the residual stress field produced by the indentation process, a more accurate experimental analysis of the hardening behavior of the 316L stainless steel used in this study will be carried out in the near future by means of some cyclic tensile-compressive tests. Once the material behavior is experimentally evaluated, the hardening behavior will be programmed into ABAQUS as a UMAT user subroutine.

Figure 19 compares the hoop residual stresses measured with contour method (CM) with the ones measured by neutron diffraction (ND). The agreement is very good in spite of the fundamental differences in the measurement methods. The good agreement further confirms the ability of each method to map residual stresses.
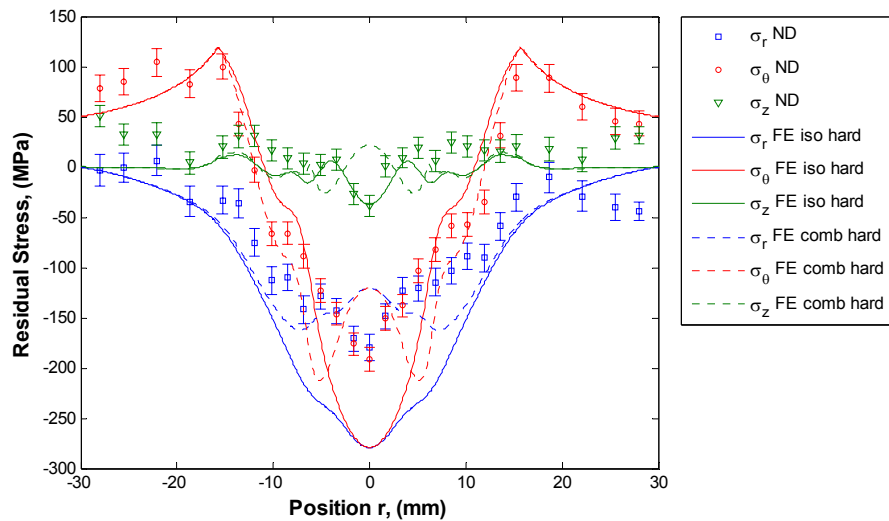
Figure 18 – *Neutron diffraction (ND) measured residual stresses plotted with the FE prediction (both isotropic and combined hardening model).*
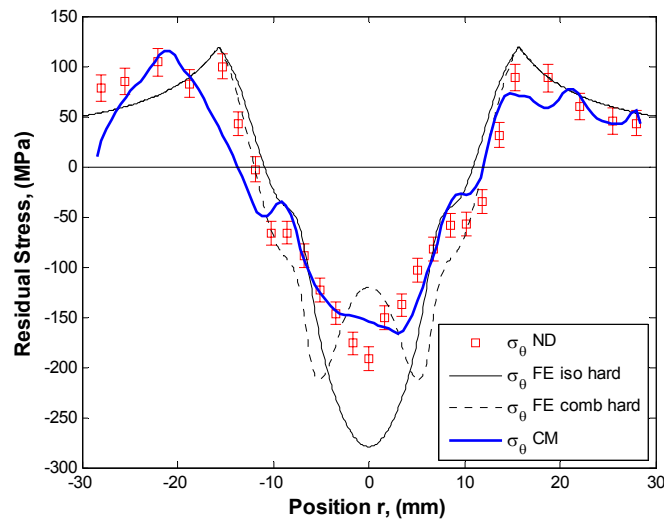

Figure 19 – *Neutron diffraction (ND) measured hoop residual stress plotted with the FE prediction (both isotropic and combined hardening model) and contour method (CM) results.*

To serve as an ideal test specimen, the stresses in the indented specimen would be calculated to sufficient accuracy with the FE model and not require independent measurement. Figure 19 indicates that the FE simulation is good but not quite accurate enough yet because of uncertainty in the hardening behavior of the material. Hopefully the accuracy will improve after cyclic testing of the 316L stainless steel. In the future, it might be more convenient to select a material with negligible Bauschinger effect so that non-cyclic constitutive testing would be sufficient for an accurate prediction.

Nonetheless, now that the residual stress field produced by the indentation process developed in this study is well known based on the neutron diffraction and contour method measurements, and in the near future to a better FE prediction, several more specimens of the same shape, extracted from the same plate (same material) and indented under the same experimental conditions (room temperature, force, cross-head speed etc.) will be produced. These specimens will be used for further experimental studies. The contour method measurement will be repeated using a larger (100 μm diameter) wire to see if a better cut can be obtained. Multiple cuts will be made to further confirm the multiple cut reconstruction theory [8]. A test will probably be mage using the slitting method to check the effects of 2-D stress variations on the usual 1-D assumption for slitting. Tests using other methods will also be considered. New specimens might be made using either finer-grained 316L or another material in order to allow x-ray measurements of stresses.

In order to validate the reconstruction theory for multiple components on this specimen, it will be necessary to apply another surface technique since the x-ray diffraction tests did not give reliable measurement because of the large grain size. The hole-drilling method used with laser speckle interferometry data [21, 22] will be applied to the measurement of the residual stresses on the cut plane.

REFERENCES

1. Prime, M.B., "Cross-Sectional Mapping of residual Stresses by Measuring the Surface Contour After a Cut," Journal of Engineering Materials and Technology, 123, 162-168, 2001.
2. Prime, M.B., "A System and Method for Measuring Residual Stress," *U.S. Patent* 6.470.756, 2002.
3. Krawitz, A.D., and Winholtz, R.A., "Use of Position-Dependent Stress-Free Standards for Diffraction Stress Measurements," Material Science & Engineering A, 185, pp.0123-130, 1994.
4. Lu, J., James, M., and Roy, G., *Handbook of Measurement of Residual Stresses*, The Fairmont Press, Inc., Lilburn, Georgia, USA, 1996.
5. Withers, P.J. and Bhadeshia, H.K.D.H., "Overview – Residual Stress Part I – Measurement Techniques," Materials Science and Technology, 17 (4), 335-365, 2001.
6. Smith, D.J., Bouchard, P.J., and George, D., "Measurement and Prediction of Residual Stresses in Thick-section Steel Welds," Journal of Strain Analysis for Engineering Design, 35 (4), 287-305, 2000.
7. DeWald, A.T., and Hill, M.R., "Multi-Axial Contour Method for Mapping Residual Stresses in Continuously Processed Bodies," Experimental Mechanics, 46(4), pp. 473-490, 2006.
8. P. Pagliaro, M.B. Prime, B. Zuccarello, "Multiple Stress Components From Multiple Cuts for the Contour Method", in Proceedings of the XXXV AIAS Conference, September 13-16, Ancona, Italy, Associazione Italiana per l'Analisi delle Sollecitazioni.
9. Mahmoudi, A.H., Stefanescu, D., Hossain, S., Truman, C.E., Smith, D.J., Withers, P.J., "Measurement and Prediction of the Residual Stress Field Generated by Side-Punching," Journal of Engineering Materials and Technology, 128, 451-459, 2006.
10. Bueckner, H.F., "The Propagation of Cracks and the Energy of Elastic Deformation," Trans. ASME, 80, pp1225-1230, 1958.
11. ABAQUS/Analysis User Manual Version 6.4, ABAQUS, Inc., 2003.
12. Choteau, M., Quaegebeur, P., Degallaix, S., "Modelling of Bauschinger Effect by Various Constitutive Relations Derived from Thermodynamical Formulation", Mechanics of Materials, 37, 1143-1152, 2005.
13. Lemaitre J. and Chaboche, J.-L., *Mechanics of Solid Materials*, Cambridge University Press, Cambridge, 1990.
14. Von Dreele, R.B., "Quantitative Texture Analysis by Rietveld Refinement", Journal of Applied Crystallography, 30, 517-525, 1997.
15. Larson, A.C., Von Dreele, R.B., General Structure Analysis System (GSAS), Los Alamos Report No. LAUR 8-748, Los Alamos National Laboratory, Los Alamos, NM, 1986.
16. Prime, M.B., Sebring, R.J., Edwards, J.M., Hughes, D.J., and Webster, P.J., "Laser Surface-contouring and Spline Data-smoothing for Residual Stress Measurement," Experimental Mechanics, 44 (2), 176-184, 2004.
17. H. Krause and A. Haase, "X-Ray Diffraction System PTS for Powder, Texture and Stress Analysis," pp. 405-8 in Experimental Techniques of Texture Analysis, DGM Informationsgesellschaft•Verlag, Oberursel 1986, H. J. Bunge, Editor.B.I.
18. C. Noyan and J. B. Cohen, Residual Stress, Measurement by Diffraction and Interpretation, Springer-Verlag, New York, 1987, (a) p. 102 (χ), (b) p. 122 and (c) p. 101.
19. TEC Model 1600 x-ray stress analysis system with SaraTEC[TM] Windows[TM] software v.1.64, Technology for Energy Corporation, 10737 Lexington Dive, Knoxville, TN 37932, www.tecstress.com.
20. D. J. Wiesner and N. R. Pappas, Residual Stress Analysis 2.0, Labview based software, ORNL, August 2006.
21. Steinzing, M. and Ponslet, E., "Residual Stress Measurement using the Hole Drilling Method and Laser Speckle Interferometry: Part I," Experimental Techniques, 27 (3), 43-46, 2003.
22. Schajer, G.S. and Steinzing, M., "Full-field Calculation of Hole Drilling Residual Stresses from Electronic Speckle Pattern Interferometry Data," Experimental Mechanics, 45 (6), pp. 526-532, 2005.